Available online at www.sciencedirect.com
ScienceDirect
Hearing Research 220 (2006) 67–75
Hearing Research
www.elsevier.com/locate/heares

Research paper

Stimulus frequency otoacoustic emissions in the Northern leopard frog, *Rana pipiens pipiens*: Implications for inner ear mechanics

Sebastiaan W.F. Meenderink *, Peter M. Narins

University of California, Department of Physiological Science, 621 Charles E. Youngdrive S., Los Angeles, CA 90095-1606, United States

Received 17 May 2006; received in revised form 3 July 2006; accepted 9 July 2006
Available online 30 August 2006

Abstract

Otoacoustic emissions (OAEs) are weak sounds that originate from the inner ear which are traditionally classified/named based on their evoking stimulus. Recently, it has been argued that such a classification, at least for mammals, misrepresents the underlying mechanisms of emission-generation. As an alternative classification, it has been suggested to recognize that OAEs arise either via nonlinear distortion or linear coherent reflection. For non-mammalian vertebrates, data on evoked OAEs that arise via the latter mechanism are largely missing. Here, we present the first measurements of stimulus frequency OAEs (SFOAEs), which are emissions thought to arise via linear coherent reflection, from an amphibian (the Northern leopard frog, *Rana pipiens pipiens*). Their properties as a function of the evoking stimulus frequencies and levels are described and subsequently compared with the previously reported properties of distortion product OAEs (DPOAEs) from the same frog species.

Keywords: Stimulus frequency otoacoustic emissions; Frog; Amphibian; Linear coherent reflection; Nonlinear distortion

1. Introduction

When a sensitive microphone is connected to the vertebrate outer ear it registers sound that arises from the inner ear. These so-called otoacoustic emissions (OAEs) may arise spontaneously (SOAEs), but they can also be evoked by broadcasting an appropriately chosen stimulus to the ear. Traditionally, OAEs are classified based on the requirement for and/or the type of the evoking stimulus. For example, OAEs have been elicited, and were named accordingly, using clicks (click-evoked OAEs or CEOAEs; Kemp, 1978), electrical stimulation (electrically evoked OAEs or EEOAEs; Mountain and Hubbard, 1989) and pure tones, either presented singly (SFOAEs; Kemp and Chum, 1980) or in combination, resulting in distortion product OAEs (DPOAEs; Kemp, 1979). In all classes of tetrapods (*i.e.* terrestrial vertebrates) one or more of these OAE-types have been demonstrated (*e.g.* SOAEs in amphibians (Van Dijk et al., 1996); reptiles (Manley, 2004); birds (Taschenberger and Manley, 1997); and mammals (De Kleine et al., 2000)). The occurrence of OAEs over the entire range of terrestrial vertebrate species suggests that their generation is a basic property of the sensory epithelium/hair cells of auditory receptors.

Within the vertebrate class Amphibia, OAEs have only been reported for the order Anura (*i.e.* frogs and toads). So far, species from the other two orders of amphibians (*i.e.* Apoda and Caudata) have not been tested for the presence of emissions. The main body of work on "frog emissions" is either on SOAEs (*e.g.* Van Dijk et al., 1989, 1996) or on DPOAEs (*e.g.* Van Dijk and Manley, 2001). Other types of evoked OAEs (SFOAEs and CEOAEs) are also found in the frog, but at present the available data on these types of emissions are limited (Palmer and Wilson, 1982; Whitehead et al., 1986).

Recently, an alternative "taxonomy" for mammalian OAEs was proposed in which emissions are classified based on their generation via either nonlinear distortion or linear cochlear reflection (Shera and Guinan, 1999). In this

* Corresponding author.
E-mail address: swfmeenderink@yahoo.com (S.W.F. Meenderink).

0378-5955/$ - see front matter © 2006 Elsevier B.V. All rights reserved.
doi:10.1016/j.heares.2006.07.009

scheme, only "pure" DPOAEs arise via nonlinear distortion, while other types of evoked OAEs (*e.g.* SFOAEs and CEOAEs) result from linear reflection of the stimulus from cochlear impedance perturbations. It should be pointed out that the linearity of the emission-generation mechanism only refers to the process by which the direction of the acoustic energy is reversed within the inner ear. This does not exclude any nonlinear mechanisms interacting with the stimulus and/or SFOAEs during their travel within the inner ear. For instance, the evoking stimulus tone and, once generated, the SFOAE have to travel within the inner ear during which they may be amplified by the "cochlear amplifier." So, even when the generation mechanism is linear, the resulting SFOAEs may exhibit nonlinear characteristics. Within the two-mechanism taxonomy SOAEs are considered reflection-source emissions that arise from intracochlear standing waves that "bounce back and forth" in the cochlea due to an impedance mismatch at the oval window and impedance irregularities in the cochlea. Although the key difference between these two types of emissions is their generation mechanism, their location of generation is also different in mammals. Whereas the generation site is fixed relative to the stimulus for distortion-source emissions (*i.e.* the generation site changes in the cochlea depending on the frequencies of the two stimulus tones), the location of the generation site for reflection-source emissions is at a fixed point along the basilar membrane, *i.e.* it is stimulus frequency independent. As a consequence, in combination with the scale-invariant tonotopic organization of the cochlea, the two different sources result in emissions that exhibit distinct phase gradients (*i.e.* different slopes of the phase versus frequency curves). As a result, the phase data obtained with OAE recordings are used as the distinguishing factor between the two types of emission sources.

To date, only few data are available on evoked reflection-source OAEs obtained in non-mammalian vertebrates (Palmer and Wilson, 1982; Whitehead et al., 1986; Manley et al., 1987; Bergevin et al., 2006). To address this lack of data, we present recordings of SFOAEs from the Northern leopard frog *Rana pipiens pipiens*. In combination with the SOAE and DPOAE data already available for amphibians, these recordings complete the data set for the two types of emissions from the mechanism-based classification in the frog.

2. Materials and methods

Stimulus frequency otoacoustic emissions (SFOAEs) were recorded from 11 ears of seven Northern leopard frogs, *Rana pipiens pipiens* ($n = 2$ female; $n = 5$ male; body weight: 19.2–40.0 g). Animals were immobilized by intramuscular injection of sodium pentobarbital solution (Nembutal; effective dosage 55–60 mg/kg body weight) in one of the hind limbs. After approximately 30 min, the anaesthetized frog was wrapped in wet gauze to prevent dehydration during the experiment and placed in a sound-attenuating chamber, the temperature of which was maintained at 24 ±2 °C.

SFOAEs were recorded using the time-domain subtraction method described by Brass and Kemp (1991). The construction of the stimulus presented using this method is illustrated in Fig. 1. Briefly, a continuous (stimulus) tone is presented to the ear at a frequency such that the stimulus tone is inverted (180° out of phase) in sections A and C relative to that in sections B and D. A second (probe) tone is presented only during sections C and D, both times with the same polarity. After recording, appropriately combining the four sections (*i.e.* A − B − C + D) results in cancellation of both the stimulus tone and the probe tone, while leaving a residual signal. This residual signal corresponds to that part of the stimulus-evoked SFOAE that is suppressed by the probe tone. When suppression in complete, it is thus equal to the stimulus-evoked SFOAE.

The stimulus tone and the probe tone were generated from the separate D/A channels (Tucker–Davis Technologies, Alachua, FL; RP2), attenuated (TDT; PA5) to set the desired levels (L_s and L_p, respectively) and presented to the frog's ear via separate insert phones (Etymotic Research, Elk Grove Village, IL; ER-2). Small plastic tubes con-

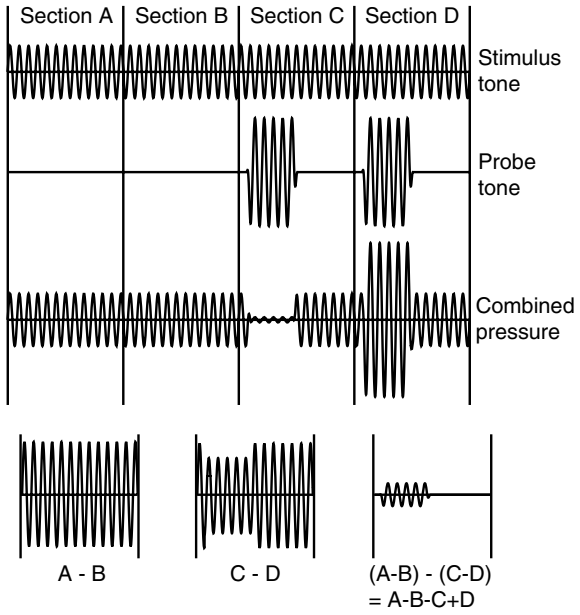

Fig. 1. Diagram showing the waveforms of the stimulus tone, the probe tone and the resulting sound pressure presented to the ear (adapted from Brass and Kemp (1991)). The continuous stimulus tone is presented at such a frequency that the waveforms in sections A and C are inverted (*i.e.* 180° phase shift) relative to those in sections B and D. The probe tone (with the same frequency but a larger amplitude as the stimulus tone) is presented as two tone bursts, with identical polarity, during sections C and D only. The combination of these tones is the resulting sound pressure presented to the subject's ear. The recorded microphone signal was segmented into the same four sections as the stimulus. The waveforms calculated from the subtraction of the microphone's sections (A − B) and (C − D) are shown. Finally, the subtraction [(A − B) − (C − D)] cancels both the stimulus tone and the probe tone from the recorded signal, but leaves a (residual) waveform representing the generated SFOAE.

nected the speakers to an ER-10A microphone system (Etymotic Research), the output of which was digitized (TDT, RP2) and stored on computer-disc for offline analysis. The stimulus and response waveforms were generated/recorded at 48.8 kHz, respectively, where both processes were controlled by customized software written in Matlab (The Mathworks Inc., Natick, MA) and Rpvds (TDT). In humans, the microphone system is inserted in the ear canal using a pliable foam tip. Since *Rana pipiens pipiens* lacks an ear canal, the foam tip was placed in a small plastic tube that was subsequently sealed to the skin surrounding the frog's tympanum using high vacuum grease (Dow Corning Corp., Midland, MI).

The stimulus parameters used in this study are summarized in Table 1. To ensure that the probe tone completely suppressed the stimulus-evoked SFOAE, its level was chosen to exceed that of the stimulus tone by as much as the dynamic range of the speakers allowed with a maximum of 20 dB. For each (f, L_s, L_p)-combination, the four segments from Fig. 1 were presented 47 times, and then averaged. Prior to averaging, each recorded microphone signal was filtered using a 400-Hz wide bandpass filter centered at the emission frequency (using Matlab routines *fir1.m* and *filtfilt.m*). Although the application of such a filter did not introduce a phase shift in the signal, it did result in a "spreading out" of the residual onset. Such spreading may bias the calculation of the waveform's time of onset (see below), thus potentially introducing error into the estimate of SFOAE onset delay. To minimize this error, the onset of the probe tone was calculated from an identically filtered signal, rather than from the electrical signal that drove the speaker, and the SFOAE onset delay was taken as the difference between the onset times of the probe tone and the residual. Additional experiments were performed with the probe sealed to a solid surface to test for nonlinear responses of the recording setup. Only for a few of the highest stimulus levels used, could small residual waveforms be discerned from the background noise. In these cases, the amplitudes of these residuals were taken as the noise floor, rather than the noise estimated from the recordings with the frog in place.

Throughout this study, the "Principles of Animal Care" (NIH-publication 85-23, revised 1985) and USA regulations were followed; all protocols were approved by the University of California Animal Research Committee.

3. Results

Stimulus frequency otoacoustic emissions (SFOAEs) were detected in all ears investigated ($n = 11$). Fig. 2a shows the first 20 ms of one residual waveform, obtained using the technique shown in Fig. 1. The SFOAE and its onset are clearly visible. For single-cycle waveform segments centered around each point in the sample, we calculated the waveform's amplitude and phase by fitting a sinusoid at the emission's frequency to the data. For comparison, Fig. 2b shows the waveform for the probe tone used to obtain this SFOAE. The waveform was calculated as the difference between sections C and A (see Fig. 1) from the recorded signal. Notice that the onset of the SFOAE waveform is somewhat delayed with respect to the onset of the probe tone. The same sinusoid-fitting procedure applied to the SFOAE waveform was used to estimate the amplitude and phase of the probe tone as a function of time. This was done because, although the voltage signals that drove the speakers had the same initial phase across frequencies, the actual stimulus phase systematically changed with frequency, resulting in a phase lag of approximately 2π at the highest frequencies tested. This phase shift was corrected in the calculation of the SFOAE group delays (see below). We calculated the amplitude envelopes of the two waveforms, using Hilbert transformations, to estimate the onset times of the respective signals (Fig. 2c). Following Whitehead et al. (1996), waveform onset was defined as the first time at which the amplitude reached 63% of its steady state value. The difference between the onset time of the probe tone and the residual was taken as the onset delay of the SFOAE. As mentioned above, the applied bandpass filter in the signal processing affects the rise time of the respective waveforms, thus biasing the estimate of onset time. By calculating the probe tone's onset time from the filtered signal, rather than from the electrical signal that drove the speaker, the effect of the bandpass filter will be the same for both waveforms and thus will not affect the derived SFOAE onset delay.

When using a constant stimulus level, SFOAE amplitude showed a bimodal dependence on frequency; relatively small emission amplitudes were found for $f \approx 1250$ Hz, while both higher and lower frequencies evoked emissions with larger amplitudes (Fig. 3). In *Rana pipiens pipiens*, this frequency has been shown to be the boundary between the

Table 1
Overview of the stimulus parameters used for the SFOAE recordings

	f_s (Hz)	Δf_s (Hz)	L_s (dB SPL)	L_p (dB SPL)	ΔL_s (dB)
SFOAE-audiograms	313 … 3015	≈30	80	$L_s + 16$	–
	313 … 3015	≈30	68	$L_s + 20$	–
	313 … 3015	≈30	62	$L_s + 20$	–
SFOAE *I*/*O*-curves	712	–	40 … 80	$L_s + 18$	2
	1013	–	40 … 80	$L_s + 18$	2
	1713	–	50 … 80	$L_s + 18$	2
	2014	–	50 … 80	$L_s + 18$	2

In all cases the probe tone frequency was equal to the stimulus tone frequency ($f_p = f_s$).

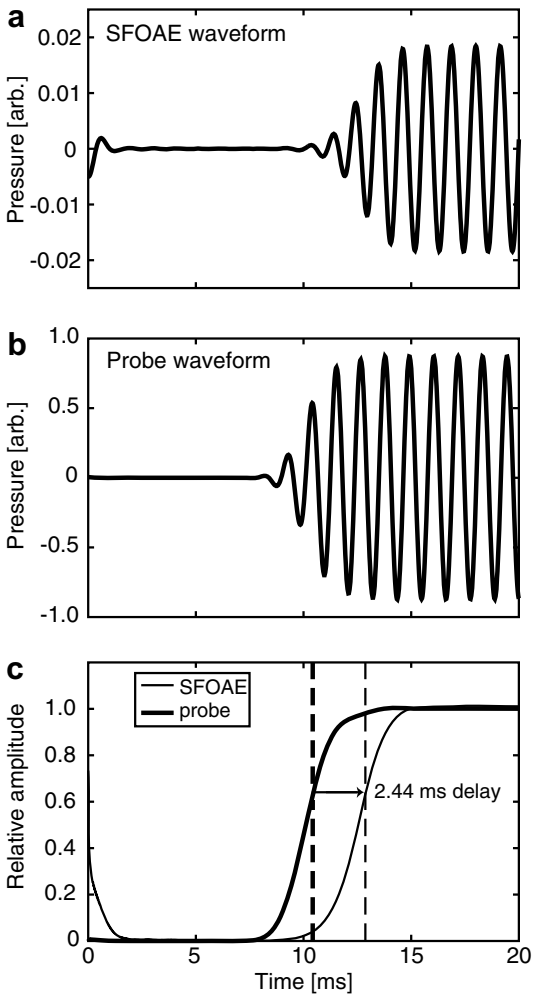

Fig. 2. First 20 ms of the waveforms for (a) the SFOAE and (b) the probe tone recorded with $f = 883$ Hz and $L_s = 80$ dB SPL. The SFOAE waveform has a delayed onset compared to the probe tone. (c) Amplitude, relative to steady state amplitude, of the waveforms in (a) and (b). The amplitude envelopes were derived from the waveform's analytical signals. As a quantitative measure for onset we determined the earliest time at which the amplitude equaled 63% of the steady state value (dashed vertical lines). The difference between these times for the SFOAE waveform and the probe waveform was taken as the SFOAE onset delay (2.44 ms in this example).

frequency ranges of highest sensitivity of the AP and the BP (Ronken, 1991). Although lowering the stimulus levels resulted in an overall decrease of emission levels, the bimodal shape of the SFOAE-audiograms was retained. The form of these SFOAE-audiograms closely resembles that of the DPOAE-audiograms recorded in the same species (*e.g.* Meenderink and Van Dijk, 2004; Vassilakis et al., 2004). For the latter, the bimodal shape is thought to reflect emission generation in either the low-frequency amphibian papilla or the high-frequency basilar papilla. Following the same line of reasoning, we suggest that SFOAEs can be generated in both auditory papillae, and that the hearing organ that contributes the largest component to the recorded emission depends on the stimulus frequency. We will refer to the emissions as either AP-SFOAEs (amphibian papilla-SFOAEs) or BP-SFOAEs (basilar papilla-SFOAEs) for emission frequencies <1250 Hz or >1250 Hz, respectively.

The phase data corresponding to the SFOAE-audiograms from Fig. 3 were used to calculate the SFOAE group delays (*i.e.* the negative slope of the phase versus frequency curves divided by 2π) after correction for the small phase shift of the stimulus tones. After unwrapping (*i.e.* removal of the discontinuities at multiples of 2π) of the phase data, the slopes were calculated as the difference in phase between adjacent samples, divided by the frequency step (which was either 32.6 Hz or 24.4 Hz, depending on frequency). Group delays were found to be very similar across ears, as well as across the three stimulus levels used (Fig. 4a). The SFOAE onset delays (Fig. 4b) derived from the waveform amplitude envelopes strongly resemble the calculated group delays. In general, the delays (both group delay and onset delay) for AP-SFOAEs were longest for frequencies between 600 Hz and 700 Hz, which corresponds to the mid-frequencies in the range of this papilla. For lower frequencies, the delays systematically decreased. Note that at these frequencies only SFOAEs evoked with $L_s = 80$ dB SPL exceeded the noise floor. A similar decrease in the delays was seen when the frequency was increased above 700 Hz, but now data are available for the three stimulus levels we used. Around 1250 Hz, the group delays were more erratically distributed. This frequency is associated with the transition from the AP to the BP, which results in "jumps" in the phase versus frequency curves. The onset delays did not show such erratic behavior around this frequency since they were not derived as a gradient (across frequencies), but rather were estimated at a single frequency. For frequencies above 1250 Hz, the delays were relatively invariant with frequency; BP-SFOAE delays did not change with changing frequency.

We evaluated the level dependence of emission amplitude by recording SFOAE input/output (I/O)-curves (Fig. 5). Although in general the SFOAE amplitude decreased with decreasing stimulus level, a clear difference can be seen in the shape of the I/O-curves from the AP and the BP, respectively (compare Fig. 5a, b versus c, d). This graphical distinction between I/O-curves from the two papillae can be quantified by expressing the slopes of the curves as a function of stimulus level. We calculated these slopes by taking the difference between adjacent points along the entire I/O-curve and dividing the difference by the stimulus level step size (2 dB). Based on the stimulus level, we distinguished between low-level slopes (stimulus level <60 dB SPL) and high-level slopes (stimulus level >68 dB SPL). Results are displayed in Fig. 6 in the form of histograms. For AP-SFOAEs, high-level emissions grew expansively (*i.e.* slope >1 dB/dB) with increasing stimulus level, while for low-level emissions from this papilla growth was compressive (*i.e.* slope <1 dB/dB). In contrast, for BP-SFOAEs the growth of emission amplitude was expansive, irrespective of the stimulus levels used.

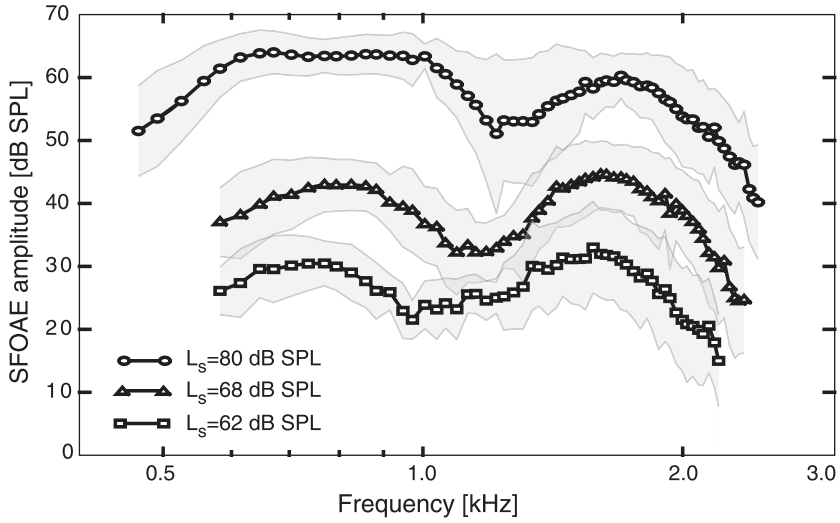

Fig. 3. SFOAE-audiograms showing the average SFOAE amplitude (±SD; shaded areas) as function of frequency combined for all 11 ears. Only data points exceeding the noise floor by at least 6 dB were included in the average. The different symbols indicate SFOAE-audiograms obtained at different stimulus levels, as indicated in the legend. Independent of stimulus level, the emission amplitude showed a bimodal dependence on frequency, resembling the response of two bandpass filters in parallel. Presumably this particular shape reflects emission generation in either the amphibian papilla ($f < 1250$ Hz) or the basilar papilla ($f > 1250$ Hz).

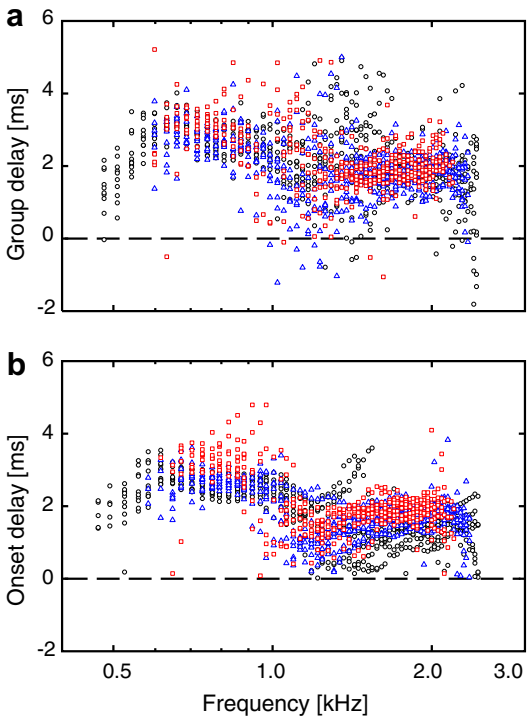

Fig. 4. (a) Group delays derived from the SFOAE phase versus frequency curves that correspond to the SFOAE-audiograms in Fig. 3. (b) Onset delays for the same data, calculated from the amplitude envelopes of the SFOAE waveform and the probe tone waveform. In both panels different symbols give the results for one of the three stimulus levels: black circles: $L_s = 80$ dB SPL, blue triangles: $L_s = 68$ dB SPL, and red squares: $L_s = 62$ dB SPL.

Also drawn in Fig. 6 are the distributions of slopes for DPOAE-*I*/*O*-curves in both papillae (adapted from Meenderink and Van Dijk, 2004), which show that the shapes of the *I*/*O*-curves are very similar for SFOAEs and DPOAEs.

4. Discussion

In this paper, we characterized stimulus frequency otoacoustic emissions (SFOAEs) from the frog ear. Anuran SFOAEs have been documented previously (Palmer and Wilson, 1982; Whitehead et al., 1986), but those data were limited to demonstrating the existence of SFOAEs in the frog. In fact, we are aware of only a few other reports of SFOAEs in non-mammalian vertebrates (Manley et al., 1987; Bergevin et al., 2006).

Anuran SFOAEs and DPOAEs exhibit several qualitative and/or quantitative similarities. Firstly, both types of OAE-audiograms exhibit a bimodal dependence on frequency, with a relative amplitude maximum below and above 1250 Hz (see Fig. 3). For DPOAEs, this bimodal shape has been interpreted as evidence for emission-generation in both the AP and the BP (Van Dijk and Manley, 2001). Likewise, we hypothesize that both papillae may generate SFOAEs and that the auditory end-organ that contributes the largest component to the recorded emission is stimulus-frequency dependent.

Secondly, OAE levels generally increase with increasing stimulus levels (Fig. 5), although *I*/*O*-curves sometimes exhibit negative slopes (“notches”) at intermediate stimulus levels. In addition, a clear difference is found between the slopes of the *I*/*O*-curves for AP- and BP-OAEs at low stimulus levels. Whereas AP-OAEs grow compressively with increasing stimulus level (*i.e.* the slope of the *I*/*O*-curve <1 dB/dB), this growth is expansive for BP-OAEs (*I*/*O*-curve slope >1 dB/dB). Not only is this dichotomy in growth between the two papillae identical for SFOAEs

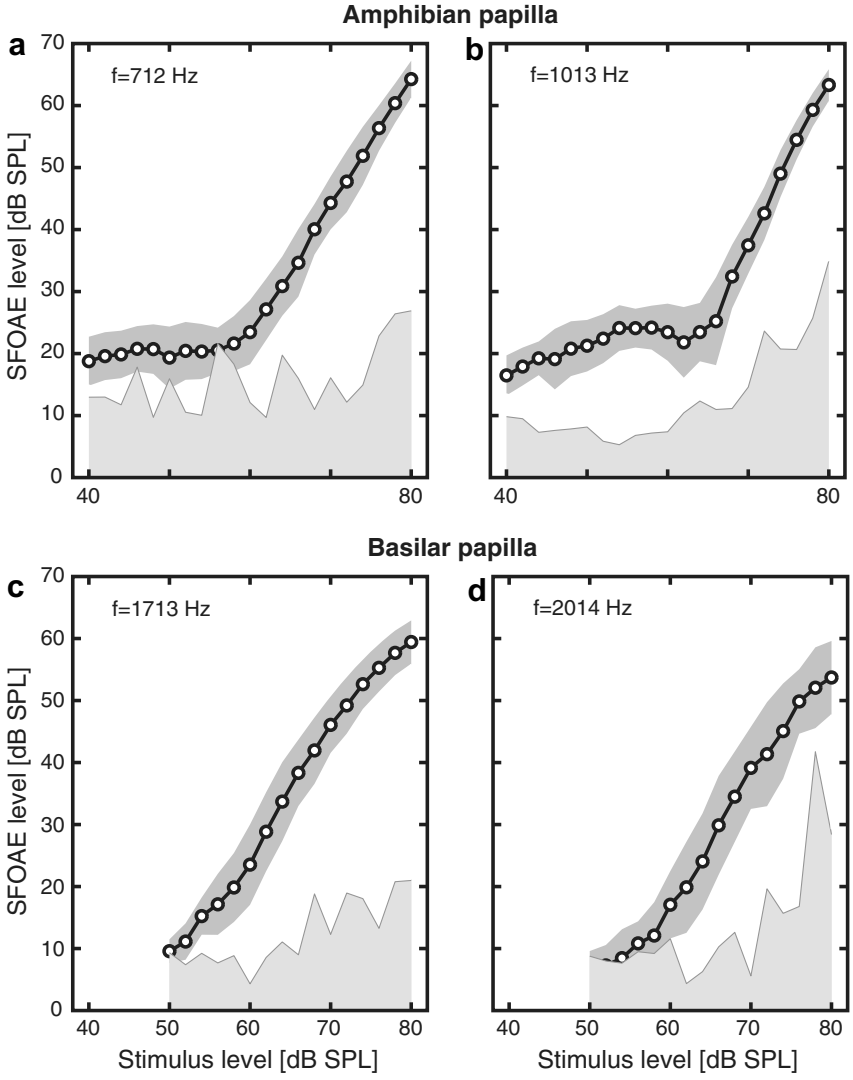

Fig. 5. Input/output (I/O)-curves for SFOAEs obtained in the amphibian papilla and the basilar papilla. Each subplot shows the mean (±SD; dark-shaded area) emission amplitude as a function of stimulus tone level at a different frequency. (a) $f = 712$ Hz, (b) $f = 1013$ Hz, (c) $f = 1713$ Hz, and (d) $f = 2014$ Hz. The light-shaded areas indicate the noise floors.

and DPOAEs, the actual slopes of the I/O-curves are also comparable for the two types of emissions (see Fig. 6). The compressive growth of low-level AP-DPOAEs, together with the presence of AP-SOAEs, have been interpreted as evidence for the presence of an inner ear amplifier in this papilla, while the contrasting properties for emissions from the BP (*i.e.* expansive growth of low-level DPOAEs and no SOAEs) have led to the hypothesis that such an amplifier is absent in the BP (Meenderink and Van Dijk, 2004, 2006). The SFOAE I/O-curves are consistent with this view.

A third similarity between anuran DPOAEs and SFOAEs is in their group delays. For both types of BP-OAEs, the delays are relatively constant around 2 ms, while they vary between 2 and 4 ms with frequency for AP-OAEs. It should be noted that whereas delays for AP-SFOAEs decrease for frequencies below 700 Hz (Fig. 4), such a trend is not as clear for AP-DPOAEs (see Fig. 3 in Meenderink et al., 2005). Rather, group delays for DPOAEs at $2f_1 - f_2$ initially decrease when $f_1 < 700$ Hz, but increase again for even lower frequencies. This may indicate a fundamental difference in generation mechanisms for the two types of emissions. However, the presented group delays for DPOAEs were obtained at different f_2/f_1 and subsequently pooled as a function of f_1. This may result in a "smearing" of the group delays across different "generator frequencies" if f_1 does not coincide with the tonotopic location of emission generation.

The SFOAE delays may provide information concerning the mechanism of acoustic energy transfer between the inner ear fluid and the auditory hair cells in the AP. The sensory epithelium of this hearing organ is more or less Ω-shaped and runs in a rostro-caudal direction within the papillar recess. The papilla is tonotopically organized, and by tracing single auditory nerve fibers with known characteristic frequencies to their point of innervation, Lewis et al. (1982) showed that this organization is along

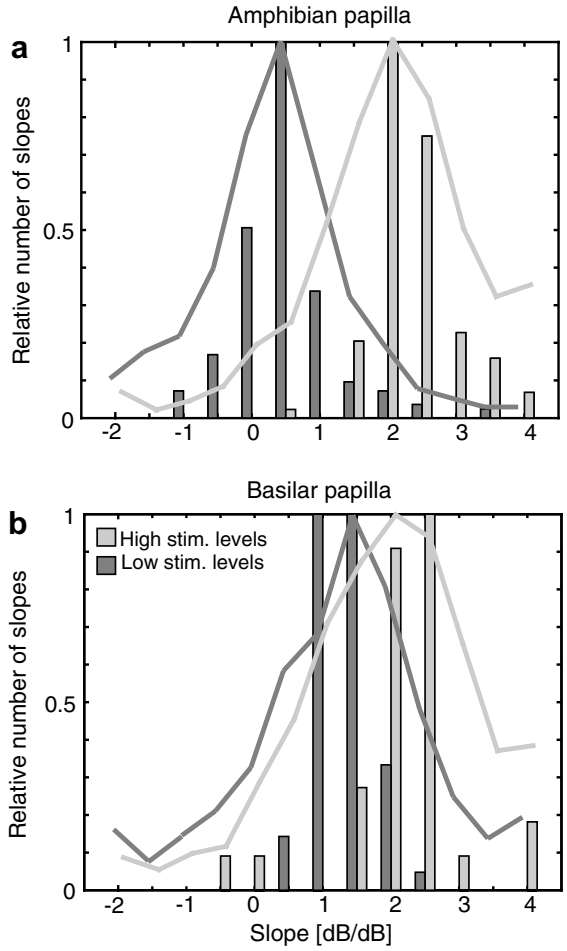

Fig. 6. Histograms showing the relative number of slopes for the SFOAE *I*/*O*-curves from Fig. 5. Results for the AP ($f = 712$ Hz, $f = 1013$ Hz) and the BP ($f = 1713$ Hz, $f = 2014$ Hz) are presented in separate panels. Each *I*/*O*-curve was divided into a high-level (L_s >68 dB SPL) and a low-level (L_s <60 dB SPL) segment. (a) Distribution of slopes at high and low stimulus levels in the AP. High-level slopes averaged 2.35 dB/dB and low-level slopes averaged 0.34 dB/dB. For reference, the solid lines show the relative number of low-level and high-level slopes for distortion product otoacoustic emission *I*/*O*-curves (adapted from Meenderink and Van Dijk (2004)). (b) Same as (a), but for SFOAEs from the BP. On average, high-level and low-level slopes were 1.67 dB/dB and 1.57 dB/dB, respectively.

the principal (rostro-caudal) axis of the sensory epithelium. Since the hair cells are directly imbedded in the cartilaginous wall of the papillar recess, acoustic energy cannot be relayed to them via the same mechanism as is found in the mammalian cochlea (*i.e.* a pressure difference between the scala media and scala tympani). Rather, it seems that the tectorial membrane (TM) that covers the hair cells plays a fundamental role in the transfer of acoustical energy to the hair bundles. Two modes of TM-excitation can be considered (Lewis and Leverenz, 1983; see also Meenderink et al., 2005). Firstly, fluid flow in the AP recess may move the so-called tectorial curtain. This is a thin extension of the TM that spans the papillar recess and connects with the papilla at the approximate location where the mid-frequencies are detected. From here, the energy may travel to other locations along the TM, thus stimulating the underlying sensory epithelium over its entire length. With this mode of excitation, hair cells tuned to the mid-frequencies will be stimulated before those that are most sensitive for lower/higher frequencies. Consequently, it may be expected that mid-frequency SFOAEs have the shortest delays, while SFOAEs with lower/higher frequencies have longer delays. In contrast, we found exactly the opposite pattern (Fig. 4), suggesting that this mode of excitation is not correct.

As an alternative mode of TM excitation, frictional coupling between the endolymph and the TM may stimulate the entire papilla as the acoustic energy "flows" through the recess. Given the small dimensions of the AP in relation to the conduction velocity of sound in water this type of endolymph-TM coupling will result in a simultaneous excitation of the entire TM. The longer SFOAE delays observed at the mid-frequencies might result from the tectorial curtain which possibly loads the TM at this location, thus providing an additional delay to the onset of the acoustically induced vibration and SFOAE generation.

For mammals, it has been proposed that SFOAEs result from linear reflection from random irregularities of the basilar membrane around the characteristic frequency of the emission (Shera and Guinan, 1999). The delays associated with these reflection-source emissions are predicted to be twice as long as the delays recorded directly at the tonotopic location of emission generation when low and moderate stimulus levels are used (Shera and Guinan, 2003). To date, recordings that are analogous to basilar membrane vibrations are not available in the frog. Evaluation of the predicted relation between the delays of such direct recordings and SFOAEs is thus not possible. However, delays of click-evoked responses in fibers of the eighth cranial nerve have been recorded in the frog (Hillery and Narins, 1987). In Fig. 7, a comparison is made between SFOAE delays (both group delays and onset delays) and these neural

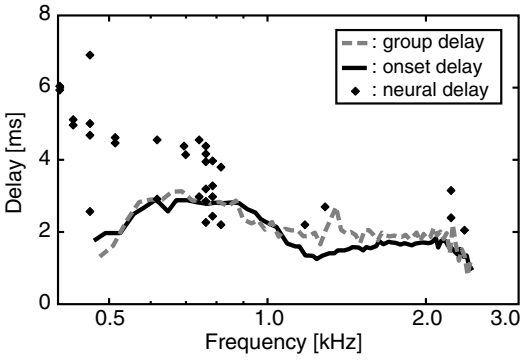

Fig. 7. Graphical comparison between SFOAE delays and neural delays. The SFOAE delays were calculated from the data in Fig. 4 as the mean across all ears and all stimulus levels (group delay: gray dashed line and onset delay: black solid line). Neural delays (black diamonds) are click latencies obtained in auditory nerve fibers of *E. coqui* or *B. orientalis* (adapted from Fig. 14 in Hillery and Narins (1987)). The observed neural delays were decreased 2 ms by these authors to correct for synaptic and neural conduction velocity delays.

delays. Although the overlap in frequencies for the obtained neural and SFOAE delays is limited, it seems evident that the SFOAE delays are not twice as long as the neural delays. It could be argued that the SFOAE delays were obtained with high stimulus levels, thus invalidating the comparison. However, the SFOAE onset delays for the *I*/*O*-curves (not shown) increase only marginally with decreasing stimulus level, suggesting that the SFOAE delays in Fig. 7 closely resemble the delays that would have been obtained at low stimulus levels. It should be noted that the discrepancy between the observed and predicted relation of the two types of delays does not exclude this particular mechanism for OAE generation *per se*. Rather, it seems to indicate that the generated SFOAEs do not propagate via a slow traveling wave in the AP.

The neural delays systematically increase for decreasing frequencies and this analogy with mammalian neural delays has been interpreted as evidence consistent with a traveling wave in the AP. Given the absence of a basilar membrane, these waves are thought to travel in the overlying TM. In the present study, we found that SFOAE delays do not exhibit a similar frequency dependence. Rather, they systematically decrease for frequencies $<$700 Hz, seemingly inconsistent with the presence of a mechanical traveling wave within this papilla. Based on DPOAE recordings, a similar observation was made by Meenderink et al. (2005).

The total neural delay between the acoustic stimulus onset and the first action potential measured in a single auditory fiber is the linear sum of three different factors: (1) the time for sound to reach and to excite the hair cell's stereovilli, (2) the time from hair bundle stimulation to action potential generation in the nerve fiber, and (3) the time for action potential propagation between the action potential generation site and the recording electrode. Similarly, SFOAE delays result from (1) the time for sound to reach and to excite the hair cell's stereovilli and (2) the time it takes for the emission to be generated and re-emitted from the ear. Since the first component is identical for the two types of delays, the difference between the low-frequency neural and SFOAE delays must be related to differences in the processes after hair bundle stimulation. If we assume that the time of SFOAE re-emission is identical across frequencies, either a frequency-dependent neural conduction velocity or an additional filtering mechanism within the hair cells must give rise to the observed difference in the low-frequency delays. Based on nerve-fiber diameter it seems that the neural conduction velocity indeed may vary with frequency (Simmons et al., 1992; Hau and Narins, 2004). But this frequency dependence would be such that the lowest frequencies have the highest conduction velocities, in contrast to the observed neural delays. As for the possibility of an additional filtering mechanism, it has been shown that anuran hair cells that are tuned to low frequencies exhibit an electrical resonance (Smotherman and Narins, 1999). Such a mechanism may very well account for the additional neural delay observed at low frequencies while not affecting the mechanically induced SFOAE delays. What is clearly lacking is a comprehensive analysis of both neural and hair cell delays coupled with an examination of the frequency dependence of spike arrival times at the dorsal medullary nucleus (cochlear nucleus in mammals).

In the present study, we characterized SFOAEs from the amphibian ear. A comparison of these data with available DPOAE data reveals several qualitative and quantitative similarities between the two types of OAEs, suggesting that they arise via a single mechanism. As such, SFOAEs can be considered as zeroth-order DPOAEs, in contrast to the current prevailing idea of two mechanisms for OAE generation in mammals.

Acknowledgement

This work was supported by NIH Grant DC-00222 to PMN.

References

Bergevin, C., Shera, C.A., Freeman, D.M., 2006. A comparative study of stimulus-frequency otoacoustic emissions in geckos and humans. Assoc. Res. Otolaryngol. Abs. 29, 24.

Brass, D., Kemp, D.T., 1991. Time-domain observation of otoacoustic emissions during constant tone stimulation. J. Acoust. Soc. Am. 90 (5), 2415–2427.

De Kleine, E., Wit, H.P., Van Dijk, P., Avan, P., 2000. The behavior of spontaneous otoacoustic emissions during and after postural changes. J. Acoust. Soc. Am. 107 (6), 3308–3316.

Hau, L.W., Narins, P.M., 2004. Auditory-nerve fiber response latencies in the northern leopard frog, *Rana pipiens*. Program No. 530.6 2004 Abstract Viewer/Itinerary Planner. Washington, DC: Society for Neuroscience.

Hillery, C.M., Narins, P.M., 1987. Frequency and time domain comparison of low-frequency auditory fiber responses in two anuran amphibians. Hear. Res. 25 (2–3), 233–248.

Kemp, D.T., 1978. Stimulated acoustic emissions from within the human auditory system. J. Acoust. Soc. Am. 64 (5), 1386–1391.

Kemp, D.T., 1979. Evidence of mechanical nonlinearity and frequency selective wave amplification in the cochlea. Arch. Otorhinolaryngol. 224 (1–2), 37–45.

Kemp, D.T., Chum, R., 1980. Observations on the generator mechanism of stimulus frequency emissions - two tone suppression. In: Van den Brink, G., Bilsen, F.A. (Eds.), Psychophysical, Physiological, and Behavioral Studies in Hearing.. Delft University Press, Delft, pp. 34–42.

Lewis, E.R., Leverenz, E.L., 1983. Morphological basis for tonotopy in the anuran amphibian papilla. Scan. Electron Microsc. (I), 189–200.

Lewis, E.R., Leverenz, E.L., Koyama, H., 1982. The tonotopic organization of the bullfrog amphibian papilla, an auditory organ lacking a basilar membrane. J. Comp. Physiol. 145 (4), 437–445.

Manley, G.A., 2004. Spontaneous otoacoustic emissions in monitor lizards. Hear. Res. 189 (1–2), 41–57.

Manley, G.A., Schulze, M., Oeckinghaus, H., 1987. Otoacoustic emissions in a song bird. Hear. Res. 26 (3), 257–266.

Meenderink, S.W.F., Narins, P.M., Van Dijk, P., 2005. Detailed f_1, f_2 area study of distortion product otoacoustic emissions in the frog. J. Assoc. Res. Otolaryngol. 6 (1), 37–47.

Meenderink, S.W.F., Van Dijk, P., 2004. Level dependence of distortion product otoacoustic emissions in the leopard frog, *Rana pipiens pipiens*. Hear. Res. 192 (1–2), 107–118.

Meenderink, S.W.F., Van Dijk, P., 2006. Temperature dependence of anuran distortion product otoacoustic emissions. J. Assoc. Res. Otolaryngol. 7 (3), 246–252.

Mountain, D.C., Hubbard, A.E., 1989. Rapid force production in the cochlea. Hear. Res. 42 (2–3), 195–202.

Palmer, A.R., Wilson, J.P., 1982. Spontaneous and evoked acoustic emissions in the frog *Rana esculenta*. J. Physiol. 324, 66.

Ronken, D.A., 1991. Spike discharge properties that are related to the characteristic frequency of single units in the frog auditory nerve. J. Acoust. Soc. Am. 90 (5), 2428–2440.

Shera, C.A., Guinan, J.J., 1999. Evoked otoacoustic emissions arise by two fundamentally different mechanisms: A taxonomy for mammalian OAEs. J. Acoust. Soc. Am. 105 (2), 782–798.

Shera, C.A., Guinan, J.J., 2003. Stimulus-frequency-emission group delay: a test of coherent reflection filtering and a window on cochlear tuning. J. Acoust. Soc. Am. 113 (5), 2762–2772.

Simmons, D.D., Bertolotto, C., Narins, P.M., 1992. Innervation of the amphibian and basilar papillae in the leopard frog: reconstructions of single labeled fibers. J. Comp. Neurol. 322 (2), 191–200.

Smotherman, M.S., Narins, P.M., 1999. The electrical properties of auditory hair cells in the frog amphibian papilla. J. Neurosci. 19 (13), 5275–5292.

Taschenberger, G., Manley, G.A., 1997. Spontaneous otoacoustic emissions in the barn owl. Hear. Res. 110 (1–2), 61–76.

Van Dijk, P., Manley, G.A., 2001. Distortion product otoacoustic emissions in the tree frog *Hyla cinerea*. Hear. Res. 153 (1–2), 14–22.

Van Dijk, P., Narins, P.M., Wang, J., 1996. Spontaneous otoacoustic emissions in seven frog species. Hear. Res. 101 (1–2), 102–112.

Van Dijk, P., Wit, H.P., Segenhout, J.M., 1989. Spontaneous otoacoustic emissions in the European edible frog *Rana esculenta*: Spectral details and temperature dependence. Hear. Res. 42 (2–3), 273–282.

Vassilakis, P.N., Meenderink, S.W.F., Narins, P.M., 2004. Distortion product otoacoustic emissions provide clues to hearing mechanisms in the frog. J. Acoust. Soc. Am. 116 (6), 3713–3726.

Whitehead, M.L., Stagner, B.B., Martin, G.K., Lonsbury-Martin, B.L., 1996. Visualization of the onset of distortion-product otoacoustic emissions, and measurement of their latency. J. Acoust. Soc. Am. 100 (3), 1663–1679.

Whitehead, M.L., Wilson, J.P., Baker, R.J., 1986. The effects of temperature on otoacoustic emission tuning properties. In: Moore, B.C.J., Patterson, R.D. (Eds.), Auditory Frequency Selectivity. Plenum, New York, pp. 39–48.